

Atomic force microscopy study of electron beam written contamination structures

M. Amman,^{a)} J. W. Sleight, D. R. Lombardi, R. E. Welser, M. R. Deshpande, M. A. Reed, and L. J. Guido

Center for Microelectronic Materials and Structures, Yale University, New Haven, Connecticut 06520

(Received 8 June 1995; accepted 23 October 1995)

Electron radiation induced hydrocarbon contamination can be either a problem or a useful tool in electron beam analyses and lithographies. We have used atomic force microscopy to study electron beam written contamination structures. Contamination is shown not only to arise from the primary electron beam but also from the energy scattered outside of the direct impingement area. The size of the contamination structures correlates well with that expected from electron scattering theory. By varying the geometry of the written structures, the rate at which the electron dose is deposited, and the nearby hydrocarbon surface density, we show that surface diffusion of hydrocarbon molecules plays a primary role in the formation of the contamination structures. © 1996 American Vacuum Society.

I. INTRODUCTION

It is well known that exposure of a surface in vacuum to an electron beam can lead to the buildup of a carbon-rich film in the exposed area.¹ This contamination is produced through electron beam induced polymerization of hydrocarbon molecules that are adsorbed onto the surface. The sources of these hydrocarbon molecules include residual hydrocarbons in the vacuum chamber and layers adsorbed onto the surface during sample preparation.² The contamination can degrade specimen images in transmission and scanning electron microscopies.³ Care must also be taken to avoid this contamination in certain electron beam lithographies. For example, patterning of oxidized silicon has been achieved by directly writing on the substrate with an electron beam and then partially etching the oxide.⁴ The presence of a contamination layer in the exposed region can interfere with this etch process. Sacrificial layers,⁵ and pre- and postexposure substrate cleaning⁶⁻⁸ have been used to address this problem. Other electron beam lithographies where contamination is an issue include selective etching of GaAs⁹ and selective area growth.¹⁰ However, contamination is not always undesirable. Electron beam written contamination structures have been used as masks for pattern transfer.¹¹ Metal lines with widths down to 80 Å have been fabricated using contamination masks.¹² Contamination is also utilized in film thickness measurements made in transmission electron microscopy.¹³

Atomic force microscopy (AFM) is a valuable technique for analyzing the topography of small structures. In this article we present the results of an AFM study of electron beam written hydrocarbon contamination structures. We discuss the size and shape of a typical structure and relate the lateral extent of the contamination to electron scattering theory. The dependence of the developed contamination on substrate material, electron dose, delay time between multiple exposures (average electron deposition rate), and writ-

ten geometry is presented. Finally, a surface diffusion picture is developed that models the observed dependencies and provides an estimate for the characteristic time of the hydrocarbon diffusion.

II. EXPERIMENTAL PROCEDURE

The hydrocarbon contamination structures were written in a JEOL 6400 scanning electron microscope modified for lithography. The exposures were made at an accelerating voltage of 40 kV and a beam current of 100 nA. Electron doses were controlled by the duration of an individual exposure and by the number of times the region was exposed. The specimen chamber was maintained at a pressure of 2×10^{-7} Torr during the exposures.

Various substrates were used in this study. These include semi-insulating and n^+ (100) GaAs, (100) GaAs precoated with 100 nm of $\text{Al}_{0.6}\text{Ga}_{0.4}\text{As}$ through metalorganic chemical vapor deposition, and p -doped (100) Si. The $\text{Al}_{0.6}\text{Ga}_{0.4}\text{As}/\text{GaAs}$ samples were grown for a separate study of InAs selective area growth on GaAs in which the $\text{Al}_{0.6}\text{Ga}_{0.4}\text{As}$ layer would be later etched away prior to the InAs growth in order to remove the electron beam induced contamination.¹⁰

After the electron beam exposure, the contamination structures were analyzed under ambient conditions using a Park Scientific Instruments atomic force microscope (AFM). Geometrical information was obtained from contact mode AFM images. The lateral sizes of the structures were typically of the order of 10 μm , while the heights were at most 200 Å. Measuring such a small height variation over a large lateral distance required a nonlinear correction during image acquisition to compensate for the AFM scanner nonlinearities. Additionally, for the images in which a significant unmodified region of the substrate was present, a second correction was performed. The correction consisted of the subtraction from the entire image of a third-order polynomial, fit to the unmodified and presumably flat regions of the substrate. No other image modifications were made.

^{a)}Present address: Engineering Division, Ernest Orlando Lawrence Berkeley National Laboratory, University of California, Berkeley, California 94720.

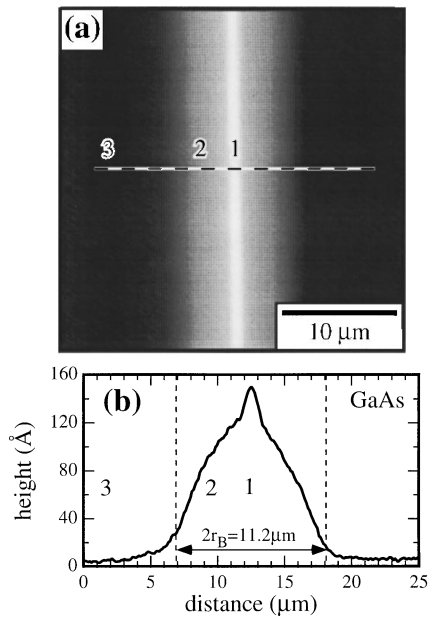


FIG. 1. (a) Atomic force microscope image of an electron beam written contamination line. The written line is 1 mm in length of which a section near the middle of the line is shown in this image. The contamination structure was created by passing the electron beam over the same vertical line (labeled 1) 40 times for a total line dose of $367 \text{ nC}/\mu\text{m}$. The regions modified indirectly by the electron beam and unchanged by the electron beam are labeled 2 and 3, respectively. The substrate is n^+ (100) GaAs. The scan size is $30 \mu\text{m} \times 30 \mu\text{m}$ with a total height variation of 151 \AA . The dashed line indicates where the cross-sectional profile shown in (b) was taken. (b) Cross-sectional profile of the electron beam written line shown in (a). Between the dashed lines is the region in which the scattered electrons interact with the substrate surface as determined from a modified electron diffusion model.

III. RESULTS AND DISCUSSION

An AFM image of a typical contamination structure written with the electron beam is shown in Fig. 1(a). The image is of a $30 \mu\text{m}$ section of a 1 mm long vertical line on a GaAs substrate. Three distinct regions are evident from Fig. 1: (1) a relatively sharp center peak, (2) a broader surrounding raised area, and (3) the unmodified substrate. The first region is in the area of direct electron beam impingement. This primary beam of electrons provides the energy necessary to polymerize the normally mobile surface hydrocarbons, creating an immobile hydrocarbon contamination structure the width of the electron beam. However, the interaction of the primary beam alone does not fully explain the observed structure. As the primary electrons enter the substrate, a number of interactions take place.¹⁴ One such interaction is the scattering of the primary electrons by the atomic electrons and nuclei of the substrate, which cause the electron beam-sample interaction region width to be larger than the beam diameter. In addition, the primary electrons may collide with the atomic electrons and ionize them, creating secondary electrons that will subsequently scatter about in the substrate. Some of the scattered primary and secondary electrons pass through the substrate surface causing further hydrocarbon polymerization. These interactions give rise to the broad contamination feature of region 2. As might be ex-

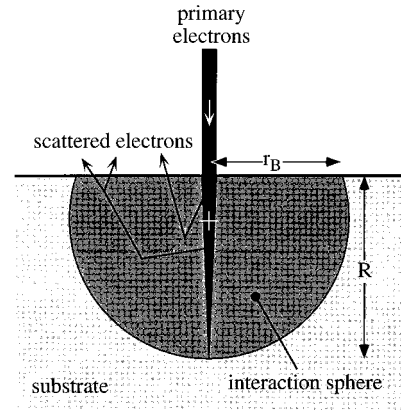


FIG. 2. Schematic cross section of an electron beam exposed solid. The primary electrons that have entered the solid are scattered by the atomic electrons and nuclei of the solid. The primary electrons can also ionize the atomic electrons giving rise to secondary electrons that scatter about in the solid. The interaction sphere is the approximate volume in which the primary and scattered electrons have energies greater than their thermal energies. The depth of this sphere into the solid is the maximum electron range R , and the radius of the intersection circle between the interaction sphere and the surface of the solid is the backscattering radius r_B . Both the incident primary electrons and the electrons scattered back through the surface can lead to hydrocarbon polymerization on the surface of the solid.

pected, the contamination is greater in the primary beam area and decreases with distance from this area due to the smaller amount of energy being deposited away from the direct impingement region. Region 3 is beyond the area of significant electron beam-sample interaction and therefore exhibits no electron beam induced contamination.

The spatial extent over which the scattered electrons interact with the substrate surface is indicated by the size of region 2. This experimentally determined interaction length can be compared to values obtained from electron scattering theory. The electron interaction volume in the substrate is approximated by a sphere that is partially contained within the substrate as shown in Fig. 2. Within this volume, the primary and scattered electrons have energies greater than their thermal energies. The quantity to be compared to the size of region 2 is the radius of the circle of intersection between the interaction sphere and the substrate surface. This is the backscattering range r_B . In the modified electron diffusion model proposed by Kanaya and Okayama,¹⁵ the backscattering range is given by

$$r_B = \frac{CR\gamma}{1+\gamma}, \quad (1)$$

where C is a parameter whose best fit value was determined to be 1.1 in Ref. 15. The maximum electron range R (μm) and the parameter γ of Eq. (1) are

$$R = \frac{2.76 \times 10^{-7} A E^{5/3} (1 + 0.978 \times 10^{-6} E)^{5/3}}{\rho Z^{8/9} (1 + 1.957 \times 10^{-6} E)^{4/3}}, \quad (2)$$

$$\gamma = 0.187 Z^{2/3}, \quad (3)$$

where Z , A (g), and ρ (g/cm^3) are the atomic number, atomic mass, and density of the substrate, and E (eV) is the energy

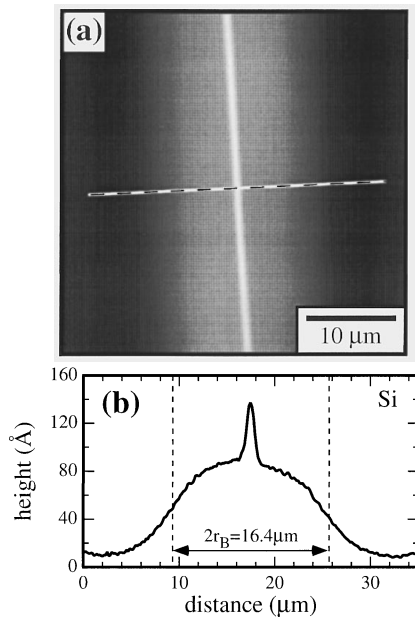


FIG. 3. (a) Atomic force microscope image of an electron beam written contamination line. The written line is 1 mm in length of which a section near the middle of the line is shown in this image. The contamination structure was created by passing the electron beam over the same vertical line 40 times for a total line dose of $367 \text{ nC}/\mu\text{m}$. The substrate is p -doped (100) Si. The scan size is $40 \mu\text{m} \times 40 \mu\text{m}$ with a total height variation of 143 \AA . The dashed line indicates where the cross-sectional profile shown in (b) was taken. (b) Cross-sectional profile of the electron beam written line shown in (a). Between the dashed lines is the region in which the scattered electrons interact with the substrate surface as determined from a modified electron diffusion model.

of the incident electrons. To apply this model to a GaAs substrate we have used atomic number and mass values that are averages of the individual elemental values. Using Eqs. (1)–(3) with $Z=32$, $A=72.32 \text{ g}$, $\rho=5.32 \text{ g}/\text{cm}^3$, and $E=40 \text{ keV}$, we obtain a value for the backscattering range of $5.6 \mu\text{m}$. This range is compared to the cross-sectional profile of the contamination line in Fig. 1(b). A dashed line is drawn on each side of the central contamination region, a distance r_B from the center peak. These lines approximately coincide with the outer edges of region 2.

The backscattering range depends in part on the physical properties of the substrate, as seen in Eq. (2). To further confirm the dependence of the contamination structure on the backscattering range, an electron beam exposure identical to that done on the GaAs substrate was made on a Si substrate. An AFM image of the resulting contamination line is shown in Fig. 3(a). From Eqs. (1)–(3) the range for Si is calculated to be $8.2 \mu\text{m}$, which is larger than that of GaAs as a result of the smaller density of Si. Hence a wider contamination line is expected and observed. The calculated value compares fairly well with the extent of the contamination as shown in Fig. 3(b). Additionally, the height of the contamination outside the direct electron beam impingement region is smaller than that observed on the GaAs sample. This is consistent with the energy of the electron beam being scattered over a larger volume in the Si sample. The energy density at the

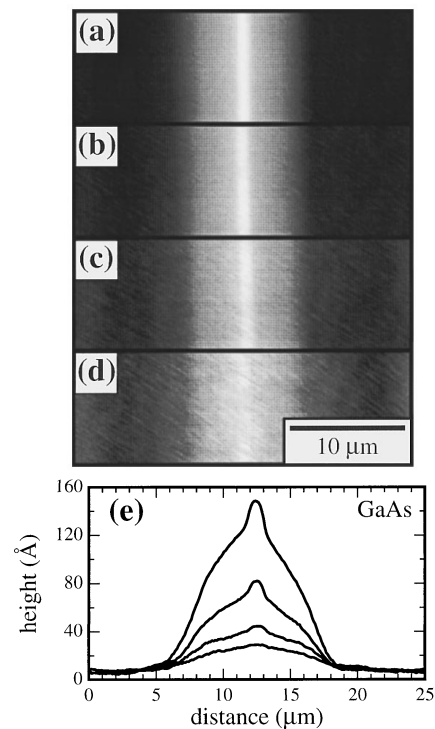


FIG. 4. Atomic force microscope images and cross-sectional profiles of electron beam written contamination lines written with various electron doses. Each line is 1 mm long of which a $10 \mu\text{m} \times 30 \mu\text{m}$ section near the middle of the line is shown. The electron dose was varied by changing the number of passes the electron beam made over the line. The substrate is n^+ (100) GaAs. The number of electron beam passes, total line dose, and total height variation for each image are: (a) 40 passes, $367 \text{ nC}/\mu\text{m}$, 149 \AA , (b) 20 passes, $183 \text{ nC}/\mu\text{m}$, 82 \AA , (c) 10 passes, $92 \text{ nC}/\mu\text{m}$, 46 \AA , (d) 5 passes, $46 \text{ nC}/\mu\text{m}$, 32 \AA . (e) Cross-sectional profiles of the electron beam written lines with the top through bottom profile corresponding to images (a)–(d), respectively. Each profile is an average of five individual line sweeps.

surface is less, and therefore a smaller accumulation of contamination results.

To achieve high electron doses, the electron beam was passed repeatedly over the exposed region. The dose dependence of the contamination structures may be conveniently studied by varying the number of electron beam passes over a given line. The results of such an experiment on a GaAs substrate are shown in Fig. 4. The images in Figs. 4(a)–4(d) are of 1 mm long contamination lines with the number of electron beam passes successively halved in going from 40 passes in Fig. 4(a) to 5 passes in Fig. 4(d). The three distinct regions identified previously in Fig. 1 are visible in each of the lines of Fig. 4. Moreover, from the cross-sectional profiles shown in Fig. 4(e), it is evident that the lateral size and overall shape of the regions remain relatively unchanged as the number of passes is varied. Each pass of the electron beam simply adds approximately the same amount of contamination to the structure as the previous individual passes, leading to the height of the contamination being proportional to the number of passes. This dependence has also been observed for similar lines written on Si substrates.

The contamination structures discussed to this point have all been relatively long, 1 mm lines. A change in the cross-

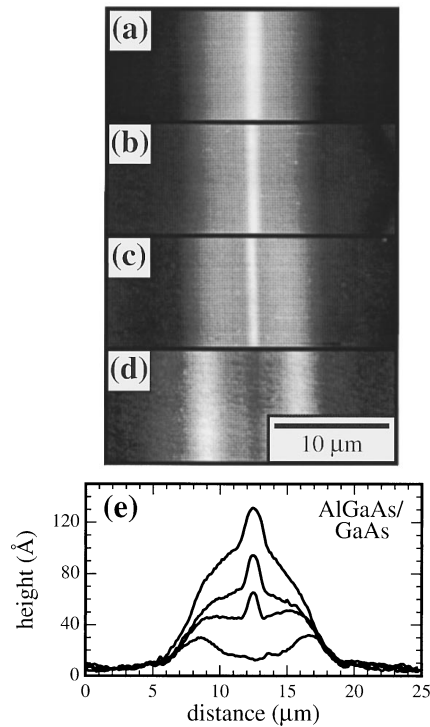


FIG. 5. Atomic force microscope images and cross-sectional profiles of electron beam contamination lines of various lengths. Each contamination structure was created by passing the electron beam over the same vertical line 40 times for a total line dose of $367 \text{ nC}/\mu\text{m}$. A $10 \mu\text{m} \times 25 \mu\text{m}$ section near the middle of each line is shown in the images. The substrate is 100 nm of $\text{Al}_{0.6}\text{Ga}_{0.4}\text{As}$ on semi-insulating (100) GaAs. The line length, time delay for the beam to return to the same point on the line τ_d , and the total height variation for each image are: (a) 1 mm , 100.2 s , 137 \AA , (b) $300 \mu\text{m}$, 30.2 s , 100 \AA , (c) $200 \mu\text{m}$, 20.2 s , 69 \AA , and (d) $50 \mu\text{m}$, 5.2 s , 37 \AA . (e) Cross-sectional profiles of the electron beam written lines with the top through bottom profile corresponding to images (a)–(d), respectively. Each profile is an average of five individual line sweeps.

sectional profile of the line occurs when the length of the written line is varied. In Fig. 5 a set of contamination lines of various lengths written on a $\text{Al}_{0.6}\text{Ga}_{0.4}\text{As}/\text{GaAs}$ substrate is shown. The images, Figs. 5(a)–5(d), are of identically written lines, except that the line lengths are varied from the longest of 1 mm in Fig. 5(a) to the shortest of $50 \mu\text{m}$ in Fig. 5(d). In the images of the longer line lengths of Figs. 5(a)–5(c), the direct impingement area, region 1, is clearly distinguishable from the surrounding broader contamination of region 2. However, as can be seen in the cross-sectional profiles of Fig. 5(e), the height of the structure decreases as the line is shortened. This decrease is not uniform, but is greatest in region 1 and lessens in moving outward into region 2. The height decrease near the center of the line cross section continues as the line is shortened until there appears to be little or no hydrocarbon contamination in this region, as is the case for the $50 \mu\text{m}$ line of Fig. 5(d). Significant contamination is still present in region 2 away from the center of the line cross section. Similar results have been obtained on GaAs without the $\text{Al}_{0.6}\text{Ga}_{0.4}\text{As}$ layer.

The change in profile with line length is a direct result of the method in which the lines are written and, additionally, provides information on the processes involved in the forma-

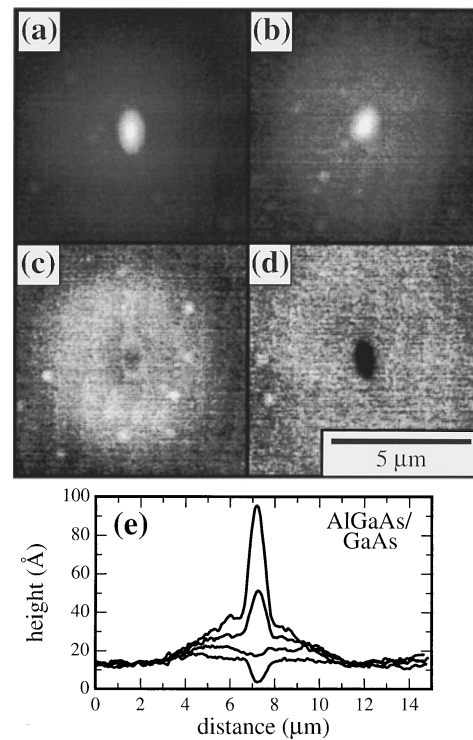


FIG. 6. Atomic force microscope images and cross-sectional profiles of electron beam written dots. Each dot structure was created by exposing the same spot 40 times for a total dose of 33.6 nC with a delay time τ_d between each of the exposures. An $8.5 \mu\text{m} \times 8.5 \mu\text{m}$ region around each dot is shown in the images. The substrate is 100 nm of $\text{Al}_{0.6}\text{Ga}_{0.4}\text{As}$ on semi-insulating (100) GaAs. The time delay between the exposures and the total height variation for each image are: (a) 2.3 s , 89 \AA , (b) 1.2 s , 46 \AA , (c) 0.7 s , 22 \AA , and (d) 22 ms , 21 \AA . (e) Cross-sectional profiles of the electron beam written dots with the top through bottom profile corresponding to images (a)–(d), respectively.

tion of the hydrocarbon contamination. As stated previously, the structures are written by passing the electron beam over the same line a number of times in order to achieve high electron doses and, as is evident from Fig. 4, to create significant contamination. The electron beam is swept at the same constant velocity along the line for all line lengths; therefore the length of the line dictates the amount of time that will elapse before the electron beam returns to the same spot on the line. This delay time τ_d is large for a long line and small for a short one. Figure 5 clearly indicates that the structure does not simply depend on the overall dose, but also on τ_d , in other words, on the rate at which the electron beam dose is deposited.

Another, simpler structure used to study the effect of the delay time is an electron beam written dot. A dot in this case is written by electron beam exposing a single spot on the substrate for a short time (approximately 8 ms), waiting a variable length of time τ_d , and then reexposing the same spot. This process is repeated until the desired electron dose is achieved. Shown in Fig. 6 is a set of dots, each written by exposing a spot on an $\text{Al}_{0.6}\text{Ga}_{0.4}\text{As}/\text{GaAs}$ substrate 40 times with τ_d being successively decreased from 2.3 s for the dot shown in Fig. 6(a) to 22 ms for the dot shown in Fig. 6(d). The long time delay contamination dot of Fig. 6(a) consists

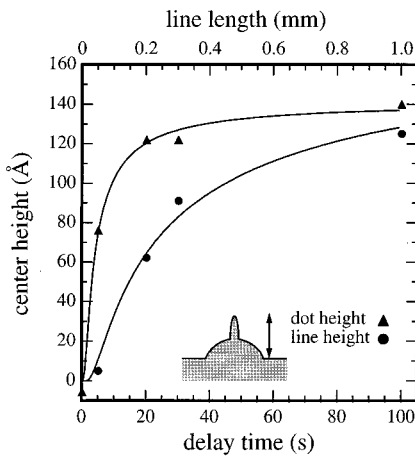


FIG. 7. Contamination height of the direct impingement region plotted as a function of delay time for both the dot and the line structures. Each structure was created by exposing the same pattern forty times for a total dose of 33.6 nC for the dots and 367 nC/ μm for the lines. The substrate is 100 nm of $\text{Al}_{0.6}\text{Ga}_{0.4}\text{As}$ on semi-insulating (100) GaAs. The solid lines are fits to the data of a model based on hydrocarbon surface diffusion.

of a relatively sharp center peak in the area of direct electron beam impingement and a broader surrounding contamination region resulting from the scattered energy of the primary beam. As the time delay is made smaller, the height of the structure decreases, as seen in Figs. 6(b) and 6(c). From the cross-sectional profiles in Fig. 6(e), it is evident that this reduction of height is greatest at the dot center, which is similar to the effect observed with the line structures.

The height reduction of the contamination structures with decreasing delay time is a direct result of the finite time required for the exposed region, reduced in mobile hydrocarbon molecules, to be replenished with molecules. In other words, the electron beam exposure temporarily decreases the number of mobile molecules in the exposed region by polymerizing the hydrocarbons and creating the observed contamination. Thus, after the exposure, the concentration of mobile hydrocarbons in the exposed region is below the equilibrium value. Hydrocarbons must then be transported to this region in order to reestablish the equilibrium concentration. The transport process requires a finite amount of time dictated by the mechanism of the transport. If the time delay is much shorter than the transport time, the exposed region becomes depleted of hydrocarbons and the structure will not grow with subsequent exposures. As the delay time is increased, however, more hydrocarbons will be present in the region of exposure prior to the event, leading to a contamination structure of greater height. If the time between exposures is much larger than the characteristic transport time, the hydrocarbon supply will replenish between exposures and the structure will grow substantially with each additional exposure. Increasing the delay time further cannot increase the quantity of hydrocarbons beyond the completely replenished equilibrium value. The contamination height, being proportional to the quantity of hydrocarbons present during the exposure, will therefore also not increase with delay time in this limit. Qualitatively this is what is observed in the line

and dot structures of Figs. 5 and 6. Plots of the center contamination height as a function of the delay time for dot and line structures are shown in Fig. 7. The structures were all written on the same $\text{Al}_{0.6}\text{Ga}_{0.4}\text{As}/\text{GaAs}$ substrate. As expected, the height of the structures increases with the delay time. The height also changes rapidly for small delay times and then appears to saturate at large times, consistent with the model.

The dependence of the contamination height on the delay time can be used to extract information on the hydrocarbon transport mechanism. Two mechanisms by which the hydrocarbons can be supplied to the exposed region are (1) diffusion along the substrate from an unexposed region, and (2) adsorption from the vacuum.² If surface diffusion is the primary mechanism, then the concentration of mobile hydrocarbon molecules can be described by the following diffusion equation:

$$\frac{\partial n(\bar{x}, t)}{\partial t} = D \nabla^2 n(\bar{x}, t), \quad (4)$$

where $n(\bar{x}, t)$ is the surface density of the mobile hydrocarbon molecules at time t and location \bar{x} , and D is the diffusion constant. The hydrocarbon density dictates in part the amount of contamination that develops during the exposure. Given the density distribution after a particular exposure $n(\bar{x}, t=0)$, the distribution that will be present at the start of the subsequent exposure $n(\bar{x}, t=\tau_d)$ can be obtained from Eq. (4). For simplicity consider the situation in which a region of the substrate is reduced in hydrocarbons from the equilibrium density n_0 to the value n_r as a result of the exposure. Applying this to both the dot and the line geometries, the following are appropriate initial conditions:

$$n(r, t=0) = \begin{cases} n_r, & 0 < r < d \\ n_0, & r > d \end{cases} \quad \text{dot}, \quad (5)$$

$$n(x, t=0) = \begin{cases} n_r, & |x| < d \\ n_0, & |x| > d \end{cases} \quad \text{line}, \quad (6)$$

where $2d$ is the effective size of the exposed region,¹⁶ and polar coordinates $\bar{x} = (r, \theta)$ and rectangular coordinates $\bar{x} = (x, y)$ have been used for the dot geometry and the line geometry, respectively. The solutions to the diffusion equation (4) assuming these initial conditions are given in the Appendix. In order to compare the two geometries, consider the time dependence of the density at the center of the exposed region, where the minimum density occurs. Letting $t = \tau_d$, the following are obtained from Eqs. (A4) and (A10):

$$n(r=0, t=\tau_d) = n_r + (n_0 - n_r) \exp\left(-\frac{d^2}{4D\tau_d}\right) \quad \text{dot}, \quad (7)$$

$$n(x=0, t=\tau_d) = n_r + (n_0 - n_r) \operatorname{erfc}\left(\frac{d}{2\sqrt{D\tau_d}}\right) \quad \text{line}. \quad (8)$$

The two solutions are plotted as a function of the dimensionless delay time in Fig. 8 for a region that is initially completely depleted, $n_r = 0$. These results, based solely on a surface diffusion source, predict the delay time dependency

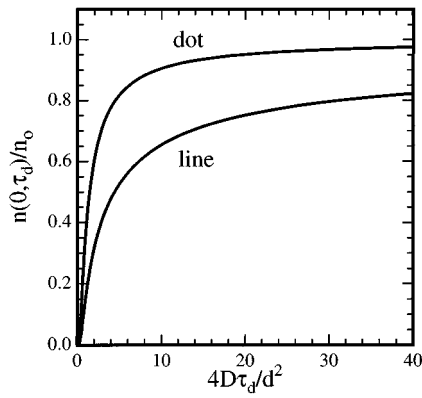


FIG. 8. Normalized hydrocarbon surface density plotted as a function of the dimensionless delay time for the dot and the line geometries. The normalized density at the center of an initially depleted region of size $2d$ is plotted. The change in density has been determined assuming only diffusion of hydrocarbons along the surface. Both normalized densities approach unity as the delay time gets large, however this occurs more rapidly in the dot geometry due to the larger hydrocarbon source available to the dot.

observed in the data of Fig. 7. At small delay times for both structures, $\tau_d \ll d^2/4D$, the density is small and therefore the accumulated contamination is small. For large delay times, $\tau_d \gg d^2/4D$, the density is near the equilibrium value, allowing significant contamination to develop during the exposure. For intermediate delay times, the measured height changes more rapidly for the dot geometry. This effect is also predicted by the simple surface diffusion model as the plots of Fig. 8 illustrate. The difference between the two geometries results from the dot effectively having a larger source of hydrocarbons to draw from and therefore recovering more quickly from the depleted state. This geometrical effect can be further illustrated by looking at the end of the $65 \mu\text{m}$ long line, shown in Fig. 9(a). The end of the line, much like the dot, effectively has a greater source of hydrocarbons than a segment far from the ends. Consequently, the line end has a greater contamination height as can be seen from the cross-sectional profiles of Fig. 9(b). The delay time dependence of the line height away from the line ends is compared to that at the line ends in Fig. 10. The greater height rise with delay time observed for the line end is consistent with the geometrical difference between the two regions. These geometrical differences would not be present if the hydrocarbons were supplied primarily by direct adsorption from the vacuum. In this simple picture, such a process would evenly coat the exposed regions.

From the simple diffusion model, we can get an estimate for the diffusion time parameter $d^2/4D$ by fitting Eqs. (7) and (8) to the data of Fig. 7. The best-fit curves, assuming $n_r = 0$, are shown in Fig. 7. The value of $d^2/4D$ is 3 s for the dots and 10 s for the lines. The difference between these two values can be partially accounted for by a difference in the size of the depleted hydrocarbon region.¹⁹ The line exposures have been effectively written with a greater dose, due to the method of exposure, and hence the scattered electron beam region has more contamination than that seen in the dot

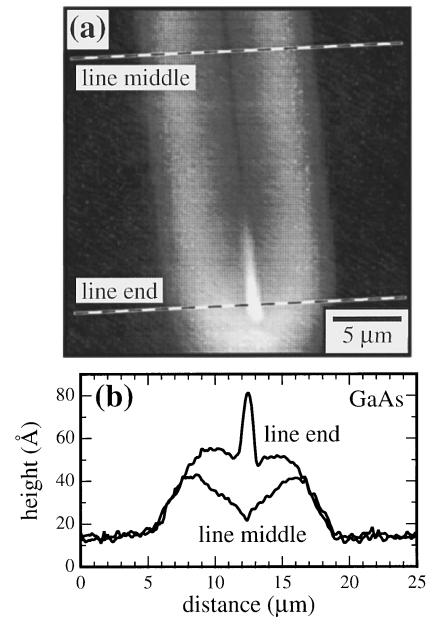


FIG. 9. (a) Atomic force microscope image of an electron beam written contamination line. The written line is $65 \mu\text{m}$ in length of which a section at the end of the line is shown in this image. The contamination structure was created by passing the electron beam over the same nearly vertical line 40 times for a total line dose of $472 \text{ nC}/\mu\text{m}$. The substrate is n^+ (100) GaAs. The scan size is $25 \mu\text{m} \times 25 \mu\text{m}$ with a total height variation of 74\AA . The dashed lines indicate where the cross-sectional profiles shown in (b) were taken. (b) Cross-sectional profiles of the electron beam written line shown in (a). The cross sections show that there is a greater quantity of contamination at the line ends as compared to regions away from the ends.

structures. The value of $2d$ is then greater for the line structures.

If the contamination growth is governed by the surface diffusion process as suggested, it should be possible to modify the growth by changing the hydrocarbon density in

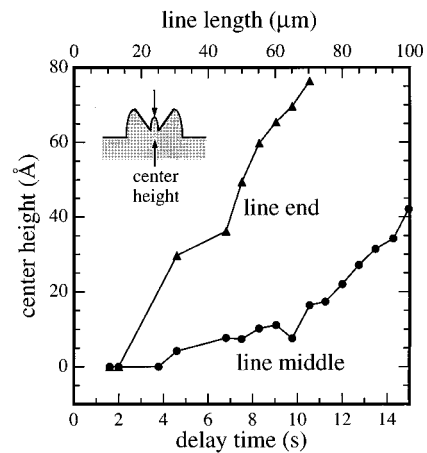


FIG. 10. Contamination height of the direct impingement region of a line plotted as a function of the delay time and line length. The height at a line end is compared to that toward the middle. Each of the line structures was written by passing the electron beam over the same line 40 times for a total line dose of $472 \text{ nC}/\mu\text{m}$. The substrate is n^+ (100) GaAs. The line end height rises more rapidly with delay time due to the larger source of hydrocarbons available to the ends.

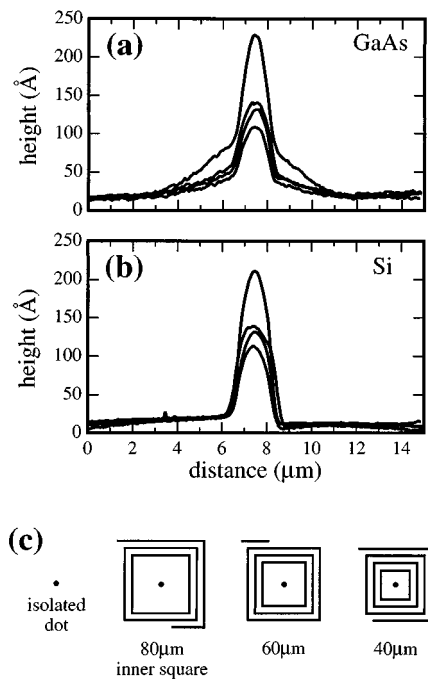


FIG. 11. (a) Cross-sectional profiles of electron beam written contamination dots obtained with an atomic force microscope. Each dot structure was written by exposing the same spot 40 times for a total dose of 33.6 nC. The delay time between each exposure was 100.2 s. From top to bottom, the profiles correspond to an isolated dot, and dots written inside concentric squares with the smallest square having a side of length 80, 60, and 40 μm , respectively. The specific patterns that were written are shown schematically in (c). The substrate is n^+ (100) GaAs. (b) Cross-sectional profiles of dots written in the same manner as those of (a). The substrate is p -doped (100) Si.

the vicinity of the written structure prior to exposure. The following experiment was performed to test this idea. The perimeters of a series of concentric squares were first written in order to reduce the hydrocarbon density surrounding a region on the substrate. Then a single dot was written in the center of the squares. The entire process was repeated until the desired electron dose at the dot was achieved. The number of squares was chosen to cause a delay of about 100 s between dot writes. The results of such an experiment performed on both GaAs and Si substrates are shown in Fig. 11. The cross-sectional profiles are of the dots written inside squares of various sizes and, for comparison, isolated dots. The heights of the dots written inside the squares are much less than those of the isolated dots. Additionally, as the squares are reduced in size, the hydrocarbon source is reduced further, causing the dot height to decrease. This is as expected from the hydrocarbon surface diffusion picture.

A final point of interest concerns the distribution of contamination for small delay times. In particular, the contamination in and near the direct electron beam impingement region (region 1) is less than that of the surrounding region (region 2) for both the line, Fig. 5(d), and the dot, Fig. 6(d). This could arise in the diffusion picture from the hydrocarbons being polymerized before they diffuse into the center of the exposed region. Hence the contamination would prima-

rily be at the edges of the exposed region. For such a process to take place, the delay time between exposures must be long enough for diffusion to occur. Based on the estimated diffusion time of 3–10 s determined earlier, this could be the case for the line of Fig. 5(d) that has an associated delay time of 5.2 s, but it is unlikely that this could explain the dot of Fig. 6(d) that was written with a very short delay time of 22 ms. Another possibility is that etching reactions begin to dominate. Carbon compounds can be etched through electron beam induced chemical reactions with adsorbed residual gas molecules, resulting in volatile compounds with carbon.^{1,2} Hydrocarbons initially present in the directly exposed region are polymerized early in the exposure cycle. As additional exposures are made, no mobile hydrocarbons are available for further polymerization. The competing etching reactions then act to remove the contamination previously created. This could take place primarily near the direct impingement region as a result of the greater amount of energy deposited in this region. A final possibility is that the exposure causes a densification of the substrate oxide. Such a densification has been previously proposed and observed for electron beam exposed silicon-oxide surfaces.^{4,7} The densification would explain the apparent pit in the direct impingement region of the dot shown in Fig. 6(d).

IV. SUMMARY

Electron beam exposure of a surface can create a buildup of hydrocarbon contamination through polymerization of surface hydrocarbon molecules. We have studied the topography of such contamination structures using atomic force microscopy. At sufficiently large electron doses, the structures are found to be larger than the area of direct electron beam impingement. Electrons scattered within the substrate and then out through the surface lead to the contamination outside of the direct impingement region. The spatial extent of contamination beyond the primary beam area has been determined from cross-sectional profiles of contamination lines written on both GaAs and Si substrates. This extent compares favorably to the surface interaction length predicted by electron scattering theory.

The dynamics of the contamination growth have been investigated by writing a pattern with the electron beam multiple times, with a controllable delay time inserted between each of the exposures. For large delay times, significant contamination results since there is sufficient time between exposures for the reduced quantity of hydrocarbons in the exposed region immediately following an exposure to be replenished before the next exposure. The quantity of contamination in this limit is proportional to the number of electron beam exposures. As the delay time is reduced, the hydrocarbon surface density has less time to recover and, consequently, less contamination is formed. For small delay times, the exposed region can become completely depleted of mobile hydrocarbons since there is insufficient time for the transport of hydrocarbons to the exposed region between exposures. The contamination structure in the direct impingement region is observed not to grow with the number of

exposures in this limit, and competing reactions that reduce the structure height may play a role. Such dependencies have been observed for both line structures in which the delay time is dictated by the line length, and dots for which an artificial delay time has been inserted between exposures.

The observed dependence of the contamination height on the delay time is consistent with a hydrocarbon surface diffusion picture. Within this picture, the hydrocarbons in the exposed region are replenished through surface diffusion of hydrocarbons from the surrounding areas. The model predicts the smaller rise in contamination height with delay time observed with the line structures as compared to that of the dots. This occurs because a section of the line away from its ends effectively has a smaller source of hydrocarbons than that of a similarly written dot. The line ends also have a greater amount of contamination than segments away from the ends for a similar reason.

The role of surface diffusion in the formation of contamination has been further illustrated by reducing the source of hydrocarbons to a region on the substrate through electron beam exposure and then writing a dot in this region. The height of such a dot is much less than that of an isolated dot, as is expected from the surface diffusion picture.

ACKNOWLEDGMENTS

The authors gratefully acknowledge the financial support of Motorola, the Advanced Research Projects Agency administered through the Office of Naval Research, the National Science Foundation through the Presidential Fellowship Program (ECS-9253760), and the NASA Graduate Student Researchers Program (NGT-50832). This material is based partially upon work supported under a National Science Foundation graduate fellowship (D.R.L.).

APPENDIX

In this Appendix the diffusion equation is solved for two different geometries: one of rotational symmetry applicable to the dot structures and the other of translational symmetry relevant to the line structures. For both cases, the situation is considered in which a single electron beam exposure reduces the equilibrium mobile hydrocarbon density n_0 by a constant amount over a region whose shape is appropriate for the structure of interest. The diffusion equation is solved in order to determine the time necessary for the reduced density region to regain the equilibrium value. Consider first the dot structure case. To take advantage of the rotational symmetry of the dot geometry, polar coordinates will be used, $\bar{x} = (r, \theta)$. If the exposed region is assumed to be circular, then $n(r, \theta, t)$ will be independent of θ and the diffusion equation (4) becomes

$$\frac{\partial n(r, t)}{\partial t} = D \left[\frac{\partial^2 n(r, t)}{\partial r^2} + \frac{1}{r} \frac{\partial n(r, t)}{\partial r} \right]. \quad (\text{A1})$$

For simplicity, further assume a region $r < d$ of reduced hydrocarbon density n_r after the exposure and no polymerization occurring outside this region. The initial condition is then

$$n(r, t=0) = \begin{cases} n_r, & 0 < r < d \\ n_0, & r > d \end{cases}. \quad (\text{A2})$$

The end of the electron beam exposure corresponds to $t = 0$. The solution to Eq. (A1) given the initial condition (A2) is²⁰

$$n(r, t) = \frac{1}{2Dt} \int_0^\infty \exp\left[-\frac{(r^2 + s^2)}{4Dt}\right] \times I_0\left(\frac{rs}{2Dt}\right) n(s, t=0) s \, ds, \quad (\text{A3})$$

where $I_0(z) = J_0(iz)$ is the zero-order modified Bessel function. The density is minimum at the center of the exposed region and is therefore the value of interest. Setting r equal to zero and using $I_0(0) = 1$, the following is obtained from Eq. (A3):

$$n(r=0, t) = n_r + (n_0 - n_r) \exp\left(-\frac{d^2}{4Dt}\right). \quad (\text{A4})$$

The analogous situation for a line structure will now be considered. If only the region of the line far from the ends is considered, the structure has translational symmetry. Using rectangular coordinates, $\bar{x} = (x, y)$, will then simplify the problem. If the y axis is chosen to be parallel to the line, $n(x, y, t)$ will be independent of y and the diffusion equation (4) reduces to the one-dimensional diffusion equation:

$$\frac{\partial n(x, t)}{\partial t} = D \frac{\partial^2 n(x, t)}{\partial x^2}. \quad (\text{A5})$$

An initial condition for a reduced density line that is analogous to that of Eq. (A2) is

$$n(x, t=0) = \begin{cases} n_r, & |x| < d \\ n_0, & |x| > d \end{cases}. \quad (\text{A6})$$

The solution to the one-dimensional diffusion equation (A5) given the initial condition (A6) is²¹

$$\begin{aligned} n(x, t) &= \frac{1}{2\sqrt{\pi Dt}} \int_{-\infty}^\infty \exp\left[-\frac{(x-s)^2}{4Dt}\right] n(s, t=0) ds, \\ &= n_r + \frac{1}{2} (n_0 - n_r) \left[\operatorname{erfc}\left(\frac{d+x}{2\sqrt{Dt}}\right) + \operatorname{erfc}\left(\frac{d-x}{2\sqrt{Dt}}\right) \right], \end{aligned} \quad (\text{A7})$$

where $\operatorname{erfc}(z)$ is the complementary error function

$$\operatorname{erfc}(z) = \frac{2}{\sqrt{\pi}} \int_z^\infty \exp(-s^2) ds. \quad (\text{A9})$$

Letting $x = 0$, the following is obtained for the density at the center of the line:

$$n(x=0, t) = n_r + (n_0 - n_r) \operatorname{erfc}\left(\frac{d}{2\sqrt{Dt}}\right). \quad (\text{A10})$$

¹J. J. Hren, in *Principles of Analytical Electron Microscopy*, edited by D.

- C. Joy, A. D. Romig, and J. I. Goldstein (Plenum, New York, 1986), Chap. 10, and references cited therein.
- ²L. Reimer, *Transmission Electron Microscopy: Physics of Image Formation and Microanalysis*, 2nd ed. (Springer, New York, 1989), pp. 457–463.
- ³K. Ura, in *Electron Beam Testing Technology*, edited by J. T. L. Thong (Plenum, New York, 1993), p. 200.
- ⁴T. W. O’Keeffe and R. M. Handy, *Solid State Electron.* **11**, 261 (1968).
- ⁵D. R. Allee and A. N. Broers, *Appl. Phys. Lett.* **57**, 2271 (1990).
- ⁶D. R. Allee, C. P. Umbach, and A. N. Broers, *J. Vac. Sci. Technol. B* **9**, 2838 (1991).
- ⁷P. E. Allen, D. P. Griffis, Z. J. Radzinski, and P. E. Russell, *J. Vac. Sci. Technol. A* **10**, 965 (1992).
- ⁸X. Pan and A. N. Broers, *Appl. Phys. Lett.* **63**, 1441 (1993).
- ⁹E. M. Clausen, J. P. Harbison, C. C. Chang, P. S. D. Lin, H. G. Craighead, and L. T. Florez, *Appl. Phys. Lett.* **57**, 1043 (1990).
- ¹⁰J. W. Sleight, R. E. Welsler, L. J. Guido, M. Amman, and M. A. Reed, *Appl. Phys. Lett.* **66**, 1343 (1995).
- ¹¹A. N. Broers, *Microelectron. Reliab.* **4**, 103 (1965).
- ¹²A. N. Broers, W. W. Molzen, J. J. Cuomo, and N. D. Wittels, *Appl. Phys. Lett.* **29**, 596 (1976).
- ¹³J. I. Goldstein, D. B. Williams, and G. Cliff, in Ref. 1, pp. 177–180.
- ¹⁴In Ref. 1.
- ¹⁵K. Kanaya and S. Okayama, *J. Phys. D* **5**, 43 (1972).
- ¹⁶The assumption of the hydrocarbon density being reduced by a constant amount over the exposed region is a simplification of the physical system. A more physically accurate reduction would be in the shape of a Gaussian or a double Gaussian (Refs. 17 and 18). However this additional complexity is not necessary to qualitatively model our data. A consequence of the simplification is that d is a quantity that is not easily extracted from the measured contamination cross sections.
- ¹⁷T. H. P. Chang, *J. Vac. Sci. Technol.* **12**, 1271 (1975).
- ¹⁸R. J. Hawryluk, *J. Vac. Sci. Technol.* **19**, 1 (1981).
- ¹⁹Other differences arise as a result of the simplifications made in the model. For example, the model does not account for the reduction of mobile hydrocarbons in the region surrounding the exposed site after many exposures. This effect is more significant for the line geometry.
- ²⁰E. Zauderer, *Partial Differential Equations of Applied Mathematics* (Wiley, New York, 1983), pp. 239, 240.
- ²¹J. R. Cannon, *The One-Dimensional Heat Equation* (Addison-Wesley, Reading, MA, 1984), pp. 32, 33.